ADVANCED FE LOWER LIMB MODEL FOR PEDESTRIANS

Yukou Takahashi
Yuji Kikuchi
Honda R&D Co., Ltd.
Fumie Mori
PSG Co., Ltd.
Atsuhiro Konosu
Japan Automobile Research Institute
Japan
Paper Number 218

ABSTRACT

The goal of this study was to develop a finite element (FE) lower limb model that can be used for direct and accurate injury prediction. Three-dimensional geometry of the lower limb bones and knee ligaments was determined from MRI scans of a human volunteer for an accurate geometry reconstruction. In order to address various loading conditions in car-pedestrian accidents, the dynamic response of the bone models was validated against the dynamic 3-point bending tests with different loading points conducted in a recent study. Material parameters for knee ligaments were determined from the latest tensile tests performed at high loading rates that may be generated in real accidents. In order to validate the dynamic response of the knee joint alone, a recently performed experiment using only the knee portion of the human subject was used. The results of these model validations showed that the model developed in this study was capable of accurately predicting the dynamic response of the lower limb bones in various loading conditions, and the dynamic shearing and bending response of the knee joint alone. It was also found that bone fracture in the 3-point bending tests and damage to knee ligaments in the shearing and bending tests can be reproduced using this model.

INTRODUCTION

A number of past studies have developed human lower limb models for pedestrians in order to reproduce lower limb injuries in car-pedestrian accidents. Bermond et al. [1][2] developed a three-dimensional FE model for the human knee joint. Although the geometry of the femur and tibia was reconstructed using a human leg X-ray scanner, direct comparison between experiment and computer simulation was not made. Yang et al. [3] developed an FE lower limb model in standing position using the DYNA3D™ program. An isotropic linear viscoelastic material representation was used for bones and ligaments. However, the geometry of the bones and ligaments was extremely simplified, and the model was validated only for the global response of the leg such as the leg acceleration in lateral impact.

More recently, Schuster et al. [4] developed an FE lower limb model that includes deformable long bones (femur, tibia, fibula) and a flat bone (patella) as well as soft tissues at the knee joint such as articular cartilage, menisci, and major knee ligaments. The geometry of the tissues came from many references, depending on anatomical regions. Although solid and shell elements were employed to represent bones, cartilage, and menisci, non-linear spring-dashpots were used for the major knee ligaments, potentially leading to difficulties in simulating the complex nature of bone-ligament and ligament-ligament contacts as well as the cross-sectional representation of the ligaments. Validation of each bone model was performed only in static mid-shaft 3-point bending. The lateral impact response of the lower limb model was validated against Kajzer et al. [5] in terms of the global response such as the knee impact and reaction forces. Bone and ligament injuries were also compared between the experiment and computer simulation. Takahashi et al. [6] developed an FE lower limb model using PAM-CRASH™ program. The geometry of bones came from the original H-Dummy™ [7], which is based on the Viewpoint Datalab™ [8]. Solid and shell elements with non-linear elastic-plastic rate dependent material characterization were used for long bones and major knee ligaments in order to accurately represent the dynamic response of these tissues as well as bone-ligament contacts. The bone models were validated against published quasi-static and dynamic mid-shaft 3-point bending test results. The knee joint response to lateral impact was validated against Kajzer et al. [9][10] with respect to the impact force, knee shear displacement, and knee bending angle. The failure of the knee ligaments

predicted in the computer simulation was compared with the experiment. Beillas et al. [11] developed an FE lower limb model designed for the application to a variety of impact scenarios. The geometry was based on MRI scans, and brick and shell elements were used to model the main knee ligaments. Again, lateral impact tests performed by Kajzer et al. [5][12] were used for validating the lateral loading response. Impact force time history was compared between the experiment and computer simulation in lateral knee shear. For lateral knee bending, time histories of impact force and leg rotation about the knee were compared.

Due to the limitation in available test results, all the bone models in these recently developed FE lower limb models were validated only in mid-shaft 3-point bending. In actual car-pedestrian accidents, however, the bumper tends to hit the proximal part of the adult leg. The material properties of the knee ligaments came directly from literature, and no validation was presented in terms of the force-deflection properties at various loading rates for each separate ligament. Regarding the lateral impact response of the knee joint, all of these recent modeling studies have used the results of a series of experiments performed by Kajzer et al. [5][9][10][12]. Since these experiments employed the entire intact limbs, the validation was limited to the overall response of the limb rather than validating the mechanical response of the knee joint alone. Apparently, one of the biggest advantages of utilizing an FE lower limb model is that the model is potentially capable of reproducing not only the global kinematic and kinetic response but also local failure of the tissues. Considering the limited validation in these currently available models, there is still a need for a more extensively validated model that is capable of reproducing more realistic impact loading scenarios for each tissue component.

In this study, the bone models were validated against the results of recently performed dynamic 3-point bending tests at three different loading points. The model for each ligament was subject to validation against the latest tensile failure tests using bone-ligament-bone complex at different loading rates. The knee joint model was validated against the experiments using isolated knee joints in order to examine the dynamic response of the knee joint alone.

MODEL DESCRIPTION

An FE lower limb model in standing position that includes the lower limb bones (femur, tibia, fibula), soft tissues at the knee joint (major ligaments, menisci, joint capsule), and muscles and skin surrounding the bony and ligamentous structures was developed using PAM-CRASH™. The geometry of the entire model was based on the MRI scans taken from a human volunteer. Material properties of bones and soft tissues were based on the previous study by the authors [6] but slightly tuned in order to better describe the latest test results.

Geometry

MRI scans of the lower limb for the femoral head and below were taken from a Japanese human volunteer at the Advanced Telecommunications Research Institute (ATR) Brain Activity Imaging Center in Kyoto, Japan. The MRI experiment was approved by the ethics and safety committee at ATR. The subject was a 35 years old male with anthropometry close to that of the AM 50th percentile (174 cm height, 78 kg weight). For bone modeling, MRI scans were performed in the transverse plane from the femoral head to the ankle at an interval of 2 mm. For the reconstruction of the smaller knee joint structures such as ligaments and menisci, it was necessary to increase the resolution of the scans. An MRI coil usually used for scanning the head region was applied to the knee region, and the scans were made in transverse, sagittal, and coronal planes at an interval of 1.5 mm. Examples of these MRI scans are shown in Figure 1 for sagittal and coronal sections around the knee joint. The scans obtained were manually processed using image processing software so that the boundary of the structure could be easily recognized. Then the boundaries of all the scans were automatically traced and three-dimensional surfaces were generated by using Forge™ software. The surface data was read into an in-house software for mesh generation.

Figure 2 shows the lower limb geometry reconstructed from the MRI scans. The model includes long bones (femur, tibia, fibula), major knee ligaments (Anterior Cruciate Ligament; ACL, Posterior Cruciate Ligament; PCL, Medial Collateral Ligament; MCL, Lateral Collateral Ligament; LCL), menisci, knee joint capsule, and surrounding muscles and skin. In our previous study, it was found that the muscles and tendons around the knee joint do not have significant effect on the lower limb response to lateral impact [6].

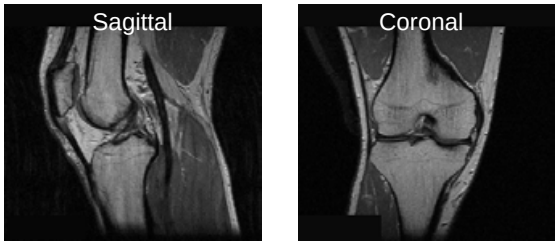

Figure 1. Example of knee MRI.

Therefore, the patella and the connecting tendon and ligament were not modeled for simplicity, and the muscles were modeled only for the padding effect in lateral impact.

The bone models consist of the cortical and trabecular layers to represent the anatomical structure of the human bones as shown in Figure 3. The trabecular layers in the epiphyses were modeled using solid elements surrounded by shell elements that represent the surface cortical layers. Although the cavity inside the cortical tubular structure in diaphysis is filled with a yellow marrow, it is a fatty tissue and its contribution to high-energy impact response was deemed negligible. The cortical tubular structure was modeled using solid elements. However, solid meshing in some metaphyseal regions resulted in very small size of elements and an unrealistically small computational time step. Thus, shell elements were applied to these areas to avoid this problem.

Three of the four major knee ligaments (ACL, PCL, LCL) were modeled using solid elements in order to accurately represent the distribution of cross sectional area as well as the ligament-ligament and bone-ligament contact (Figure 4). Shell elements were selected for the MCL considering its thinness. The cruciate ligaments (ACL, PCL) are considered to have two bundles with different orientation and mechanical response [13]-[15]. In order to take this into account, the ACL and PCL models were divided into two bundles (Anteromedial ACL bundle; A-ACL, Posterolateral ACL bundle; P-ACL, Anterolateral PCL bundle; A-PCL, Posteromedial PCL bundle; P-PCL) as shown in Figure 5. The insertion sites were estimated from anatomy CD-ROMs [16][17], and were rigidly attached to the corresponding bony surface areas. The inferior surface of the menisci was attached to the tibial plateau using the tied contact in PAM-CRASH™ (sliding interface definition type 32) [18][19]. The entire knee joint was covered by the joint capsule modeled using shell elements (Figure 4).

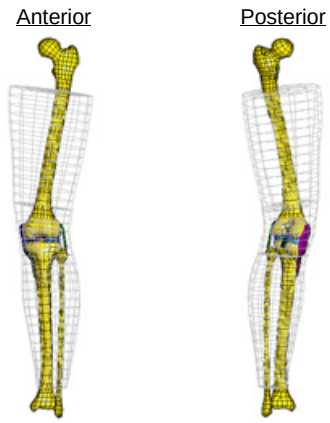

Figure 2. Geometry of FE lower limb model.

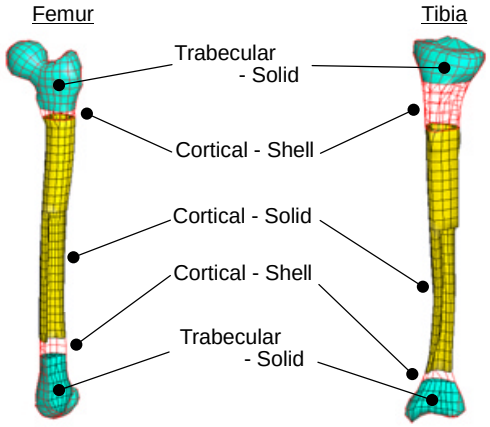

Figure 3. Structure of bone models.

Material Property

Material properties for bones and soft tissues were based on a previous study by the authors [6] and will not be repeated here in detail. Non-linear elastic-plastic rate dependent material characterization was used for

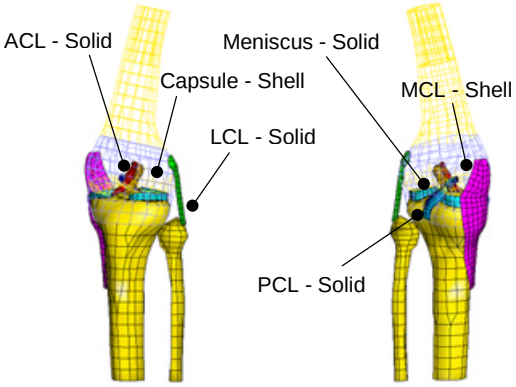

Figure 4. Models for knee ligaments and menisci.

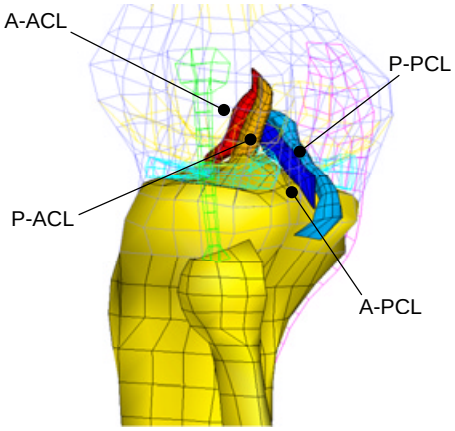

Figure 5. Models for ligament bundles.

bones, ligaments, joint capsule, and skin. Material types 16 and 105 were chosen for solid and shell elements, respectively. Strain rate dependency of the constitutive relationship was modeled using the curve definition function with logarithmic interpolation and the Cowper-Symonds strain rate law for the bones and soft tissues, respectively. Material modeling for the flesh padding came directly from H-Dummy™ [7], which employs a non-linear viscoelastic material model (material type 22). In our previous study, trilinear stress-strain curves were used for ligaments to simulate the initial slack region, subsequent elastic region, and plastic region. The validation process for each individual ligament bundle is described below, however, it was difficult to simulate the plastic region in the force-deflection response at various loading rates using the trilinear stress-strain representation. For this reason, bilinear representation (initial and elastic) was used and the damage parameters in material type 16 and 105 were introduced. These values were determined so that the plastic region of the force-deflection response predicted by the model would best represent that from the experiment. It is known that the meniscus behaves elastically during a high-speed impact [20]. Based on this finding, it was decided that the material property of the menisci be modeled using elastic material model. Material parameters for bones and ligaments were slightly tuned from our former study through the model validation. It was not possible to find data sources for the material properties of the knee joint capsule. Thus, the material properties of the skin determined in our previous study were used as an initial estimation, and were tuned in the knee joint model validation described below.

MODEL VALIDATION

The lower limb model with geometry from the MRI scans and material properties estimated from our previous study was subject to validation against a series of recent experiments.

Bones

Model Setup

The bone models were validated at different loading points against dynamic 3-point bending tests for the femur, tibia, and fibula in the lateromedial direction performed at the University of Virginia, Center for Applied Biomechanics (CAB) [21]. The bones were potted in potting cups with rollers at their distal and proximal ends. The roller part of the potting cup was placed on the support plate, and the support load was measured by a load cell placed underneath the plate. The ram had a circular tip and was rigidly attached to a servo-hydraulic test machine. The rigid ram was used for femur bending. However, in order to minimize the potential local failure at the ram-bone interface, Confor™ foam was applied to the ram for the tibia and fibula bending. The ram was displacement controlled at approximately 1.5 m/s, and displacement transducers were used to monitor the force-deflection response. For each bone, three loading points were used – mid-shaft, proximal third, and distal third, resulting in nine setups (three bones at three different loading points).

These nine setups were represented using the FE bone models. As an example, the model setup for the tibia mid-shaft loading is presented in Figure 6. The boundary of the support plates, modeled using shell elements, was rigidly fixed to the inertial space. The

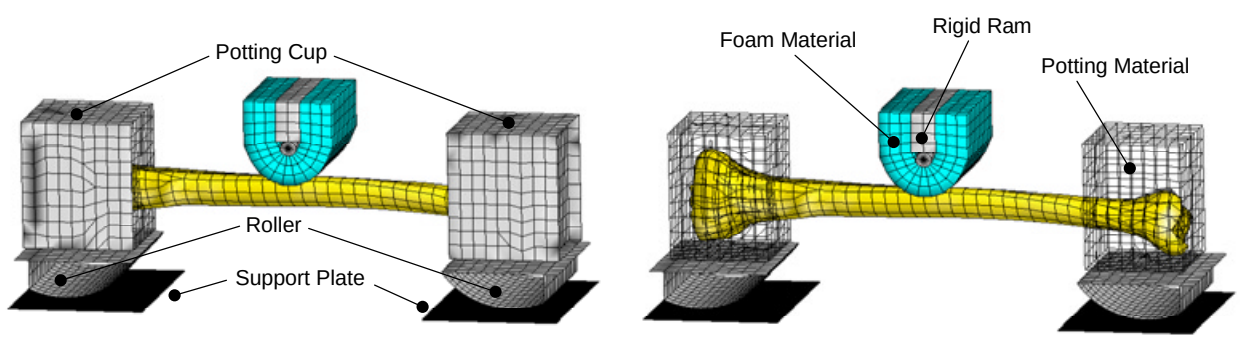

Figure 6. Schematic diagram of tibia mid-shaft 3-point bending model.

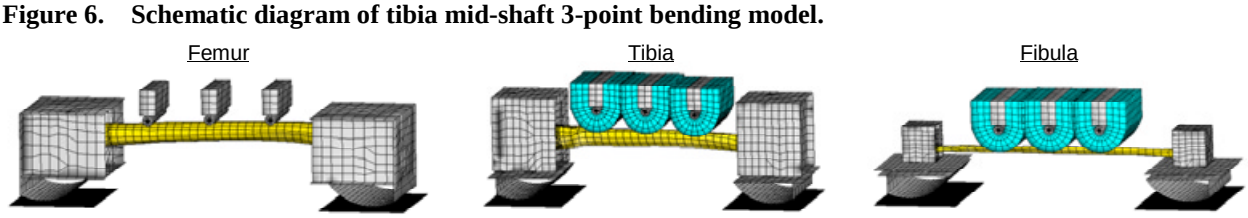

Figure 7. Model setups for 3-point bending of femur, tibia, and fibula.

potting cups with rollers were also modeled with shell elements. Inside the cup, the space between the epiphyseal region of the bone and the potting cup was filled with solid elements, representing the potting material used in the experiment. The ram was modeled as a rigid body, and the displacement time history of the ram was prescribed using the average time history from the experiment. For the tibia and fibula tests, the rigid ram was surrounded by the foam modeled using solid elements. Material property of the foam was determined based on Darvish et al. [22]. Figure 7 displays the model setups for the femur, tibia, and fibula. The rams at mid-shaft, proximal and distal third were superimposed in one bone model setup. Potting cups with different sizes were utilized among the three different bones.

Results

The time sequences of the bone bending to failure for all of the nine test setups simulated using the FE model are presented in Figure 8. The element elimination option in PAM-CRASH™ was specified in order to simulate and graphically display the failure of the bone.

Force-deflection and moment-deflection responses to failure were compared between the experiment and computer simulation in Figure 9 and 10, respectively. The tests were performed using one, two, or three specimens, depending on the test conditions. The blue curve(s) and the red curve represent the results of the test and the computer simulation, respectively. In order to compensate for the variety in anthropometry of the specimens, the test results were scaled using the scale factors for force (λ_F), moment (λ_M), and displacement (λ_D) defined in Equations (1)-(3)

$$\lambda_F = (\lambda_L)^2 \quad (1).$$
$$\lambda_M = (\lambda_L)^3 \quad (2).$$
$$\lambda_D = \lambda_L \quad (3).$$

where λ_L is the length scaling factor. By recognizing that the mass scale factor, λ_{mass}, is proportional to λ_L^3, both mass and height of the human subject can be taken into account by introducing an equivalent length scaling factor, λ_{Lequiv}, defined in Equation (4).

$$\lambda_{Lequiv} = (\lambda_{mass}\, \lambda_L)^{1/4} \quad (4).$$

Scale factors were determined using the length of each bone model (femur; 46.7 cm, tibia; 39.1 cm, fibula; 35.6 cm) and the weight of the full body model (74.6 kg) as developed in the previous study by the authors [6].

At the timing of failure, the force sharply dropped for both the experiment and computer simulation, allowing the force and displacement magnitude to be easily compared from these graphs. For all loading locations in the femur bending, computer simulation results showed a relatively sudden rise in force at the initial stage, which is not present in the test results. This discrepancy is not observed for the tibia and fibula. A possible explanation for this is that the foam was not applied to the ram for the femur, and the ram was assumed to be completely rigid in the computer simulation. This may have resulted in an unrealistically stiff contact between the ram and the bone surface prior to the bone deflection. However, the purpose of the bone model validation was to look at the validity of the force-deflection response of the bone rather than precisely simulating the experiment. Therefore, it was decided to compare the stiffness and the magnitude of force and deflection at failure, and the discrepancy at the initial stage was deemed not important. From this viewpoint, the simulation results exhibited a good match with the experimental results, suggesting that the bone models can accurately reproduce the dynamic stiffness and failure properties of the actual bones.

Ligaments

Model Setup

The models for the six ligament bundles from the four major knee ligaments were validated against quasi-static and dynamic tensile tests to failure performed at CAB [23]. From the knee joint of a human cadaver, bone-ligament-bone complex was taken in order to preserve the insertion sites. The specimen was anatomically oriented so that the knee was straight, representing the standing posture of a pedestrian. The distal and proximal ends of the specimen (bone part) were potted, and the distal potting cup was rigidly fixed. The proximal potting cup was rigidly attached to the displacement controlled servo-hydraulic test machine and was pulled up along the long axis of the tibia quasi-statically and dynamically. Three different loading rates were used – 1 mm/min (quasi-static), 160 mm/s (medium rate), and 1600 mm/s (high rate). Thus, the resulting test cases should be eighteen (three loading rates for six ligament bundles). Unfortunately, this test program is still ongoing and the results for only a part of these eighteen cases were currently available. Table 1 shows the combination of the ligament bundles and loading rates for which the test results were currently available.

The FE models for the distal part of the femur and the proximal part of the tibia-fibula complex, as well as each ligament bundle, were used for simulating these tests. Since the bone is much stiffer than the ligament bundle, all the bones were assumed to be rigid in order

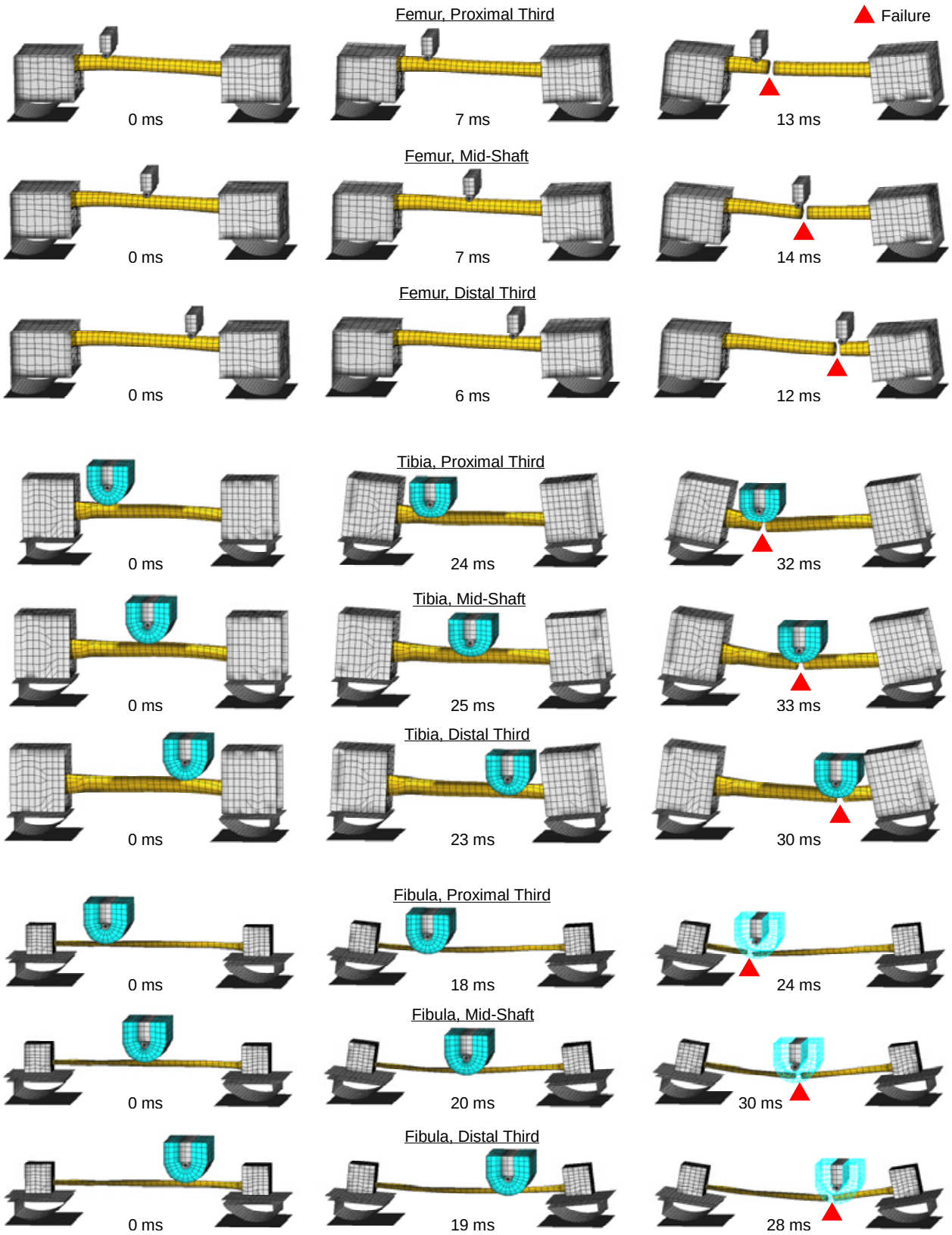

Figure 8. Time sequences of bone bending for proximal third, mid-shaft, and distal third loading. For fibula, foam is displayed as wire frame so that failure sites are visible.

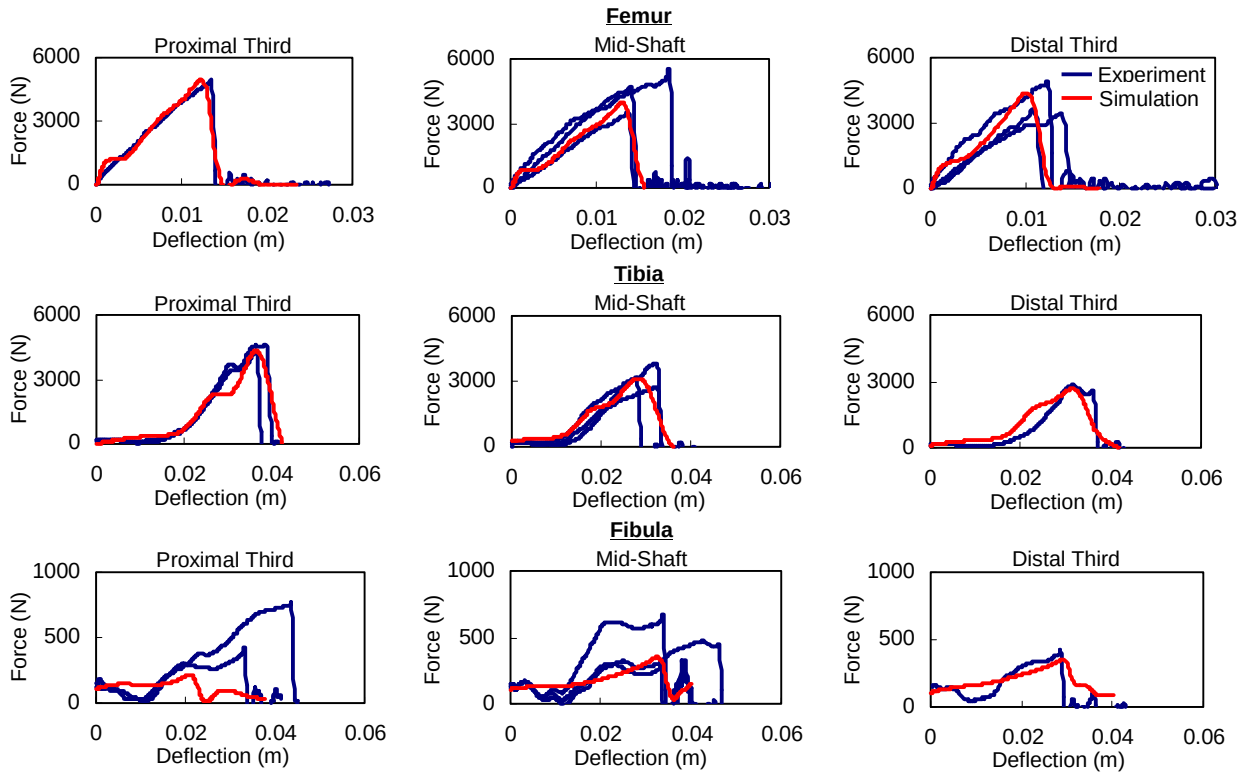

Figure 9. Comparison of force-deflection response to failure between experiment and computer simulation in dynamic 3-point bending.

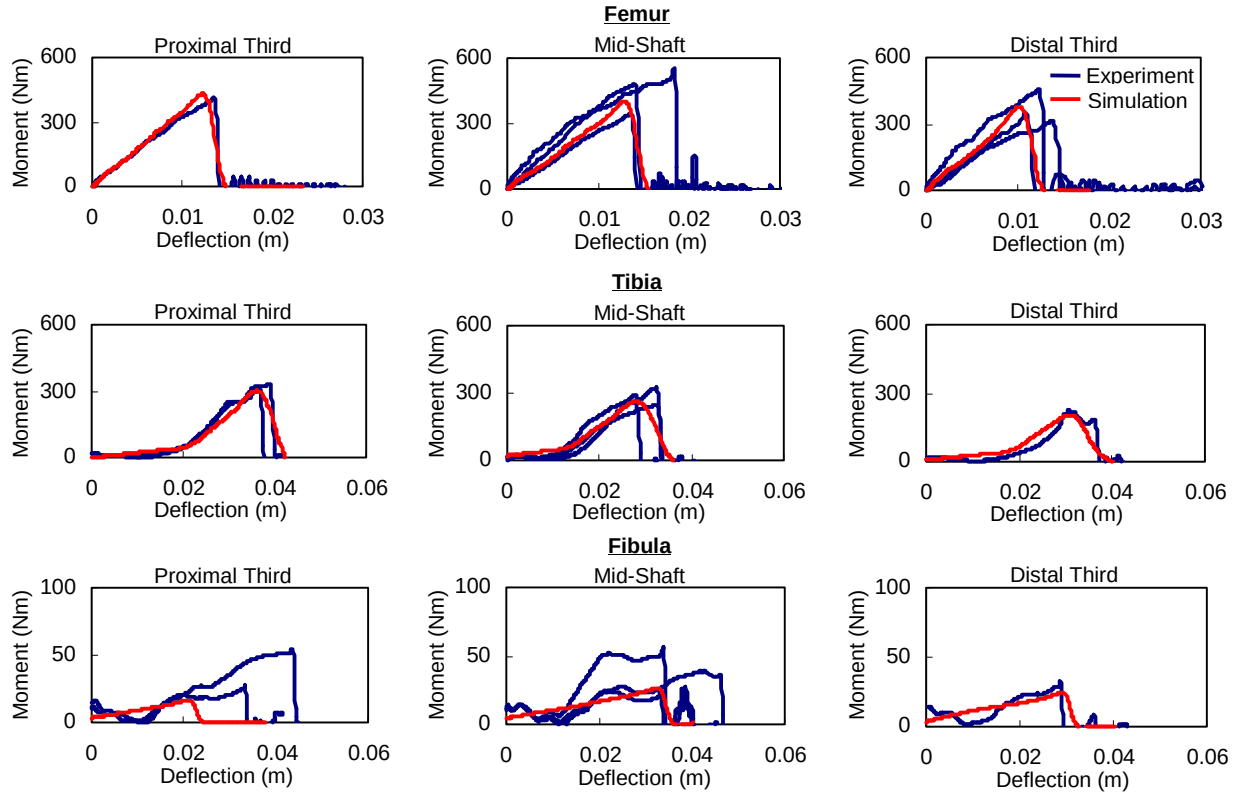

Figure 10. Comparison of moment-deflection response to failure between experiment and computer simulation in dynamic 3-point bending.

to minimize the CPU time. At the superior and inferior insertion sites, the ligament bundle was rigidly attached to the corresponding bones. The rigid tibia-fibula complex was fixed to inertial space, and the upward motion of the femur was prescribed using the average displacement time history of the fixture from the corresponding tests.

Results

Figure 11 illustrates the time sequences of the ligament kinematics to failure for the eight test cases for which test results were available. For quasi-static tests in this figure, displacement was noted rather than

Table 1.
Test conditions for which test results were available

	Quasi-static (1mm/min)	Medium Rate (160mm/s)	High Rate (1600mm/s)
A-ACL		■	■
P-ACL	■		
A-PCL	■		
P-PCL			■
MCL	■		
LCL	■	■	

■ available

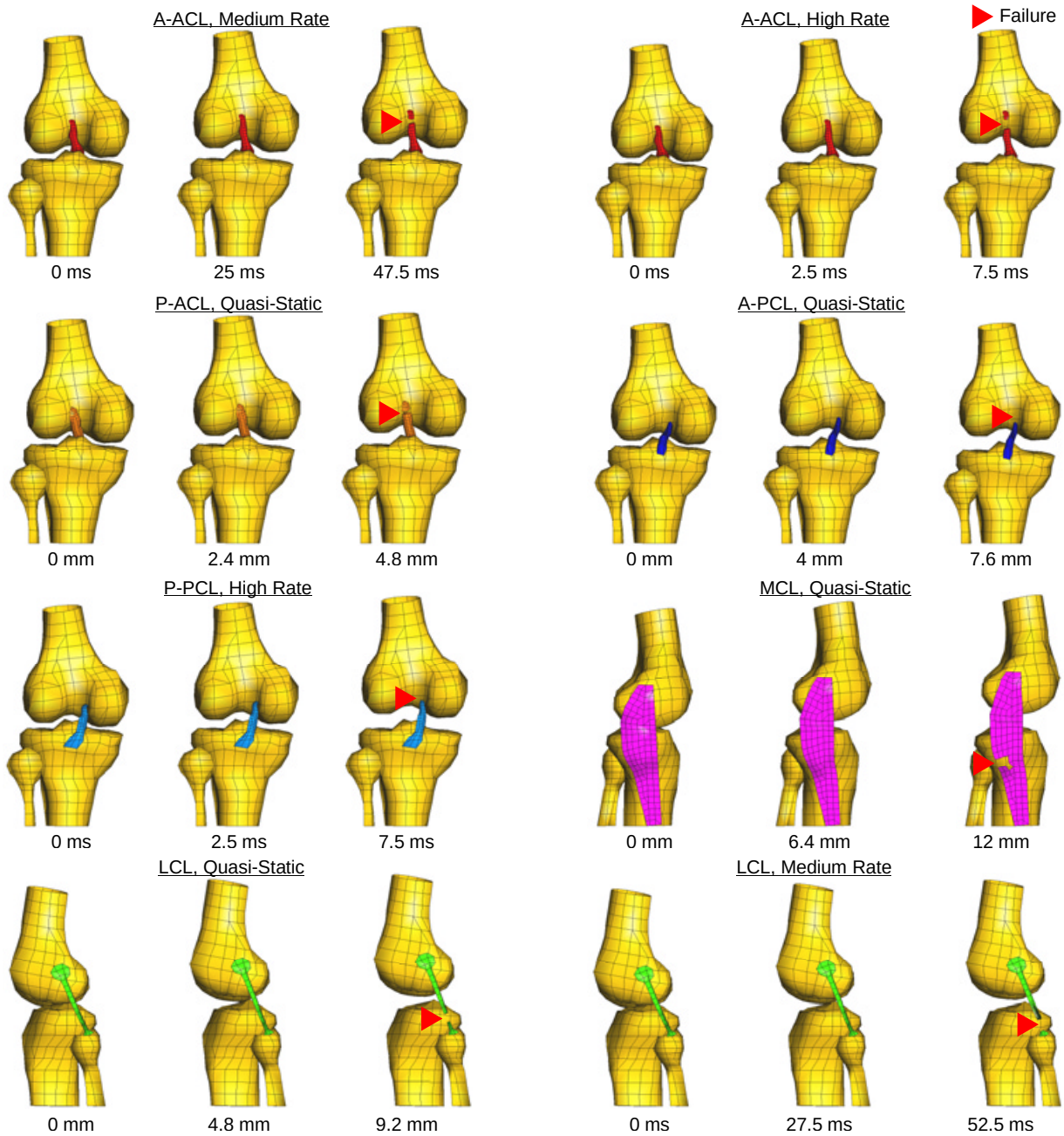

Figure 11. Time sequences of ligament tension to failure.

time. Again, element elimination option in PAM-CRASH™ was used in order to simulate and graphically illustrate the failure of the ligament bundle. It should be noted that the bone-ligament-bone complex was in anatomical orientation simulating the standing position of the knee joint, and the femur was pulled up along the long axis of the tibia. This resulted in a loading direction different from the long axis of the ligament bundles.

The force-deflection response obtained from the computer simulation was compared with that from the experiment in Figure 12. The blue and red curves in the graphs represent the results of the test and computer simulation, respectively. For the first step, the ligament

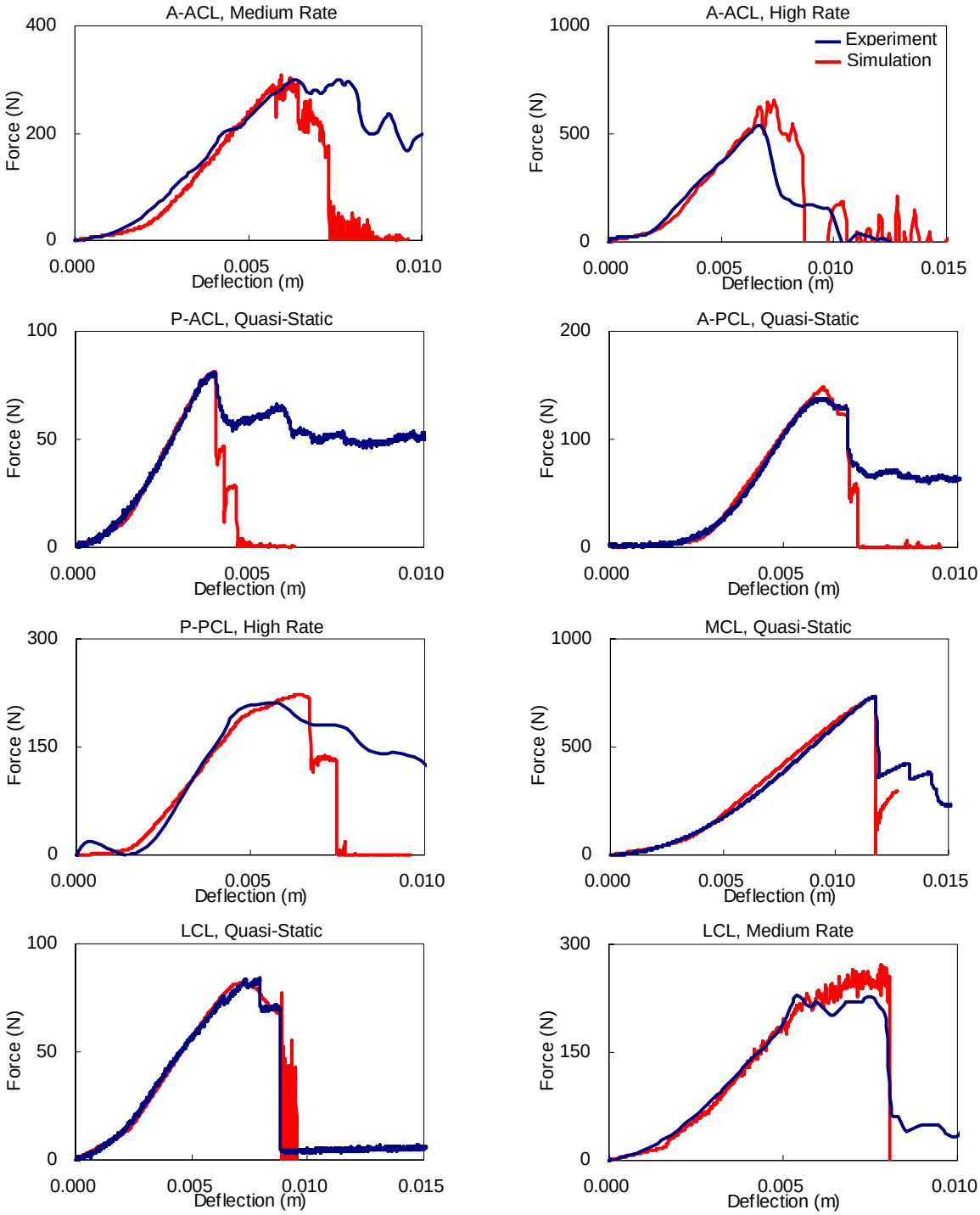

Figure 12. Comparison of force-deflection response to failure between experiment and computer simulation in quasi-static and dynamic tensile tests.

bundles for which quasi-static test results were available (P-ACL, A-PCL, MCL, LCL) were validated to determine their quasi-static stress-strain relationships. Since the quasi-static test results were not available for the A-ACL and P-PCL, it was necessary to estimate the quasi-static stress-strain relationship for these ligament bundles. For A-ACL and P-PCL, the quasi-static constitutive models determined for the P-ACL and A-PCL, respectively, were used as an initial estimation, and were slightly tuned in order to obtain a better match to the test results in dynamic conditions. Strain rate parameters of the Cowper-Symonds strain rate law for A-ACL, P-PCL, and LCL were determined in the validation at medium and/or high loading rates. In some cases, test results did not show a sharp drop in force after failure. This may be due to a gradual propagation of the fibrous rupture, which cannot be simulated using a model with a small number of elements in the cross section. However, for the purpose of predicting the risk of ligamentous damages in car-pedestrian impact, the stiffness before failure and the force and elongation at failure are much more important as compared to the force-deflection property after failure. In terms of the stiffness and failure properties, all comparisons presented in Figure 12 showed very good agreement between the experiment and computer simulation.

Knee Joint

Model Setup

Dynamic bending and shearing tests of the knee joint using isolated knees from human cadavers run by CAB [21] were computationally simulated using the FE knee joint model. In the experiment, the proximal and distal ends of the knee (bone part) were potted in potting cups. The overall length of the specimen was determined so that all of the insertion sites of the ligament bundles could be kept intact. In order not to destroy the knee joint structure, all the tissues around the knee joint were maintained. For potting purposes, however, the flesh around both ends of the specimen was removed. The potting cups were connected to load cells and subsequently to the end boxes. In bending tests, the end boxes provided a one-dimensional rotational degree of freedom in the coronal plane as well as a one-dimensional translational degree of freedom in the superoinferior direction. The fork with two circular tips was connected to a servo-hydraulic test machine through a pin joint in the coronal plane. The fork was pushed dynamically against the end boxes in the lateromedial direction. As the distance between the two tips of the fork was shorter than that distance between the initial position of the pin joints at the end boxes, this configuration provided 4-point bending of the system. 4-point bending ideally applies a constant bending moment and no shear force between the two loading points. In shearing tests, the end box on the proximal side was only allowed to translate in the superoinferior direction, and a constant axial force of approximately 850 N was applied in this direction. The end box on the other side was rigidly attached to the servo-hydraulic test machine which provided lateromedial motion of this part. The fork was displacement controlled at a peak velocity of approximately 1 m/s, and the distal end box in shearing tests was also displacement controlled and was targeted at a constant velocity of approximately 1.5 m/s.

Figure 13 shows schematic diagrams of the model setups representing the bending and shearing tests. All the parts of the test apparatus were modeled as rigid bodies except for the end boxes. The end boxes were modeled as deformable in order to accurately represent the contact between the tips of the fork and the boxes. These rigid parts were connected to each other using rigid joint elements. The mass, center of gravity, and moment of inertia for each part were separately calculated and were given to each rigid body. The bony part of the specimen inside the potting cups was rigidly connected to the cups. Other than this region, the entire specimen was modeled as deformable, including bones and soft tissues. In the model for the specimen, the distal part of the femur, proximal part of the tibia-fibula complex, six ligament bundles, menisci, and joint capsule were included. Although the flesh around the knee was maintained in the experiment, it was decided not to include the flesh model for simplification since the flesh was dissected and the mechanical contribution of this part was deemed much smaller when compared with that of the ligaments and joint capsule. In the bending setup, the joints connecting the proximal and distal end boxes to the inertial space were allowed to rotate in the coronal plane as well as to translate in the superoinferior direction as shown in Figure 13. In the shearing setup, the joint at the proximal end box was allowed to translate in the superoinferior direction, while the lateromedial motion of the distal end box was prescribed based on the average displacement time histories from the experiment. Constant axial compressive force of 850 N was applied to the proximal end box for the shearing setup.

Results

Figure 14 shows the time sequences of the knee joint kinematics to ligament failure for both bending and shearing setup. Element elimination option in PAM-CRASH™ was used to represent failure of the knee ligament bundles.

The stiffness of the knee joint was compared

between the experiment and computer simulation by plotting the moment-angle and force-displacement responses in the bending and shearing setups, respectively (Figure 15). The same scaling technique employed for the bone test results was applied to the knee joint test results except for the length scale factor (λ_L), which was determined using the height of the full body model (176 cm) developed by the authors [6]. The test results show a relatively large variation for both of these plots. However, it could be confirmed that the trend of the simulation results was similar to that of the experiment, and the order of the stiffness magnitude from the simulation was within the variation of the experimental results, suggesting that the knee joint stiffness in bending and shearing was reasonably estimated using this model.

Ligamentous damage at the knee joint in the bending and shearing setups is shown in Figure 16, and is compared between the experiment and computer simulation in Table 2 and 3, respectively. In the bending setup, rupture of the MCL was observed in all the test cases, which was also predicted in computer simulation. In one out of three bending tests, the ACL partially ruptured. In our computer simulation, the ACL remained intact. In shearing setup, only ACL rupture took place in the tests, and the computer simulation also predicted the ACL failure. No other ligament was damaged in both the experiment and

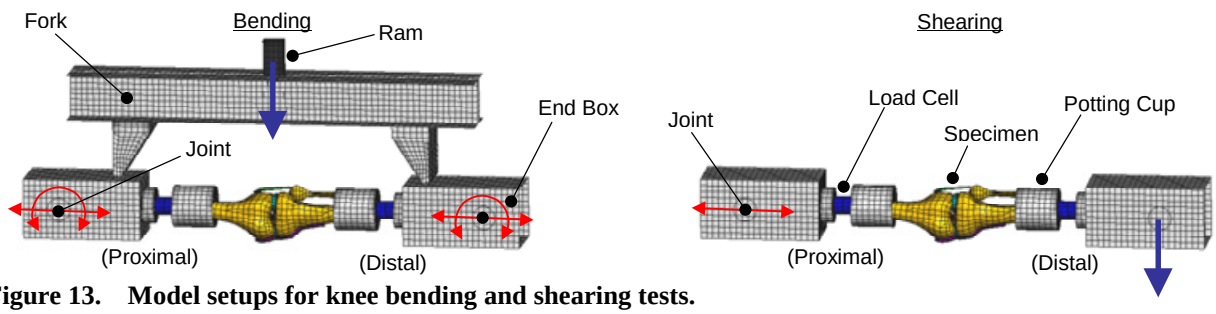

Figure 13. Model setups for knee bending and shearing tests.

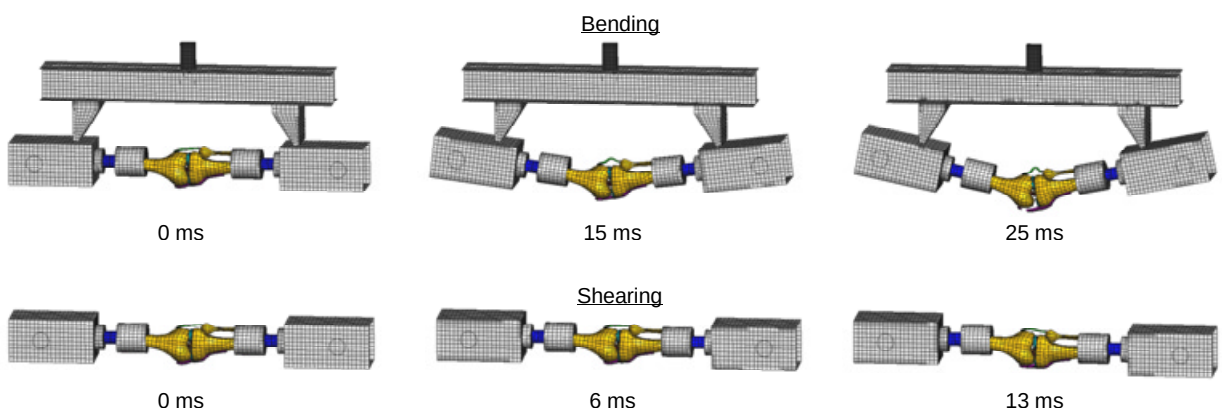

Figure 14. Time sequences of knee bending and shearing to ligament failure. (joint capsule is not shown)

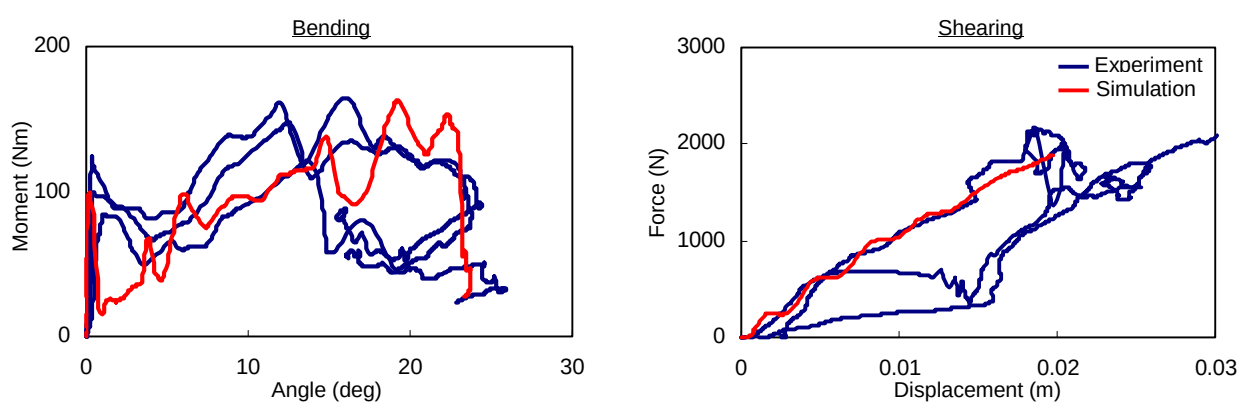

Figure 15. Comparison of knee joint stiffness between experiment and computer simulation.

computer simulation.

DISCUSSION

The bone models developed in this study used the material properties based on a previous study by the authors [6]. In order to better describe the risk of bone fracture, material properties in tension were used, since it is believed that bone often fails in tension. One of the reasons why the bone models were validated against the experiment with different loading points was that it allowed the significance of anisotropic nature of the bone material properties to be estimated. However, good correlation between the experiment and computer simulation in terms of the force-deflection and failure properties could be obtained by using isotropic material characterization. This suggests that the anisotropy of the bone material properties may not play a significant role on determining the stiffness and failure properties in 3-point bending.

The latest ligament test results enabled the model for each ligament bundle to be validated at different loading rates. However, this series of tests is still ongoing and the only ligament bundle for which both quasi-static and dynamic results could be obtained was the LCL. For the LCL, it was not possible to match the dynamic results only by applying a strain rate model for the quasi-static material properties. It seemed that not only stress, but also strain, was rate dependent. Since the current material modeling only takes into account the rate dependency of the stress, the strain at failure was slightly changed between the quasi-static and dynamic simulation. Therefore, the model developed in this study was tuned to better describe the

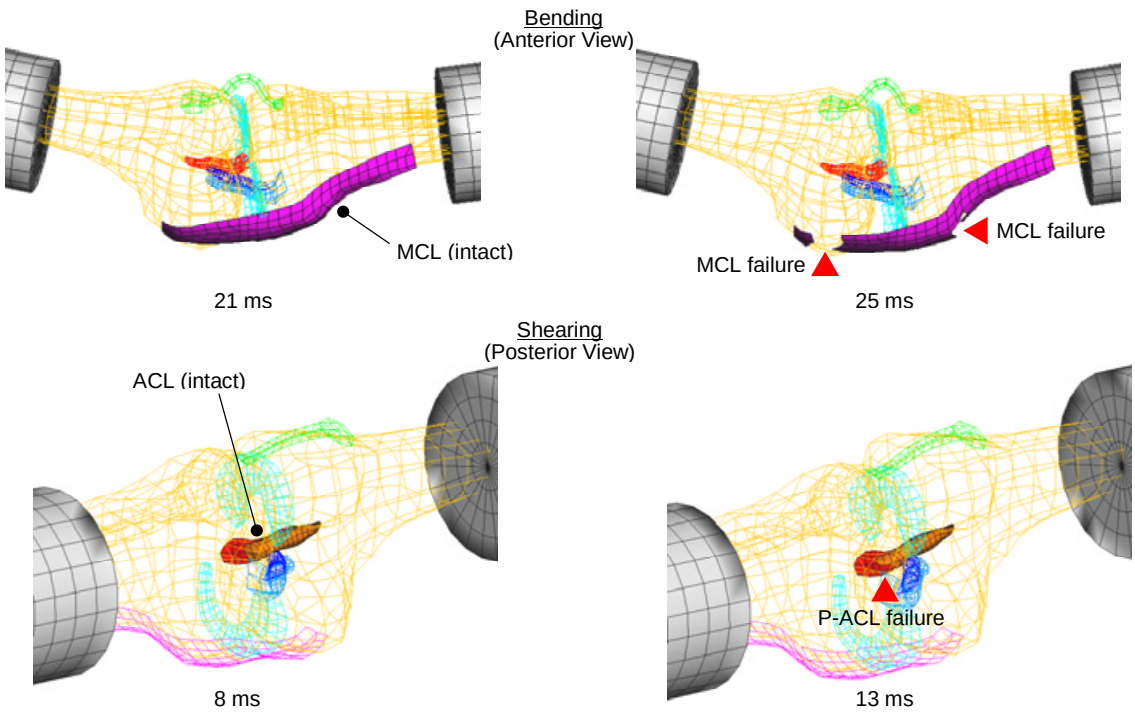

Figure 16. Ligamentous damage in bending and shearing simulation.

Table 2.
Comparison of ligamentous damages in knee bending between experiment and simulation

	Test #1	Test #2	Test #3	Computer Simulation
ACL		■		
PCL				
MCL	■	■	■	■
LCL				

■ Ligament failure

Table 3.
Comparison of ligamentous damages in knee shearing between experiment and simulation

	Test #1	Test #2	Test #3	Computer Simulation
ACL	■	■	■	■
PCL				
MCL				
LCL				

■ Ligament failure

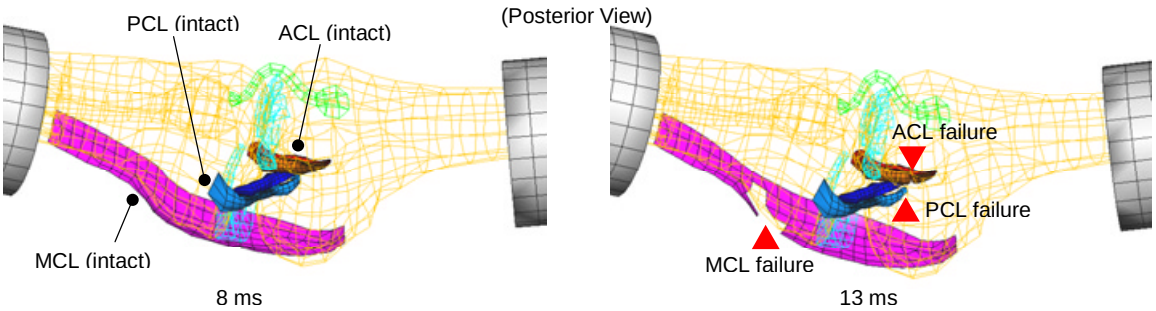

Figure 17. Ligamentous damage in knee bending simulation without joint capsule.

dynamic response of the tissues, rather than the quasi-static response. In order to cover a wider range of loading rates, more complete descriptions of the rate dependency of material properties are needed.

When simulating the knee bending and shearing tests, it was necessary to include the model for the joint capsule, in order to obtain good results for both the joint stiffness and the injury prediction. Figure 17 shows the ligamentous damage in the bending setup predicted using the model without the joint capsule. Without the capsule, the PCL with no damage in the tests ruptured, while force-deflection response of this ligament was validated. This may suggest that the joint capsule is one of the major contributors that determine the mechanical response of the knee joint. The material properties of the joint capsule should be further investigated.

CONCLUSION

An advanced FE lower limb model for a pedestrian was developed using MRI scans from a human volunteer. The bone models were validated against dynamic 3-point bending test results at different loading points, and the results showed that the model can accurately predict the force-deflection response as well as failure properties.

Each ligament bundle was subject to validation against tensile tests to failure at different loading rates in terms of the force-deflection and failure properties. The results showed that the model can accurately predict the dynamic responses. However, it was found that not only stress, but also strain should be rate dependent. More advanced material models should be used in order to develop a model that can be applied to wider range of loading rates.

The knee joint validation showed that the model could predict the dynamic stiffness and failure properties of the knee joint alone. It was found that the joint capsule might have a significant roll on the mechanical response of the knee joint.

The results of these extensive validations suggest that the model developed in this study can be used for understanding injury mechanisms of the pedestrian lower limb as well as for developing appropriate tools and injury criteria for evaluating injuries to the pedestrian lower limb in real-world car-pedestrian accidents.

REFERENCES

[1] Bermond F., Ramet M., Bouquet R., Cesari D., “A finite element model of the pedestrian knee-joint in lateral impact”, IRCOBI, 1993.

[2] Bermond F., Ramet M., Bouquet R., Cesari D., “A finite element model of the pedestrian leg in lateral impact”, 14th ESV, 1994.

[3] Yang J.K., Wittek A., Kajzer J., “Finite element model of the human lower extremity skeleton system in a lateral impact”, IRCOBI, 1996.

[4] Schuster P. J., Chou C. C., Prasad P., “Development and Validation of a Pedestrian Lower Limb Non-Linear 3-D Finite Element Model”, Stapp Car Crash Journal, Vol. 44, 2000-01-SC21, 2000.

[5] Kajzer J., Cavallero C., Ghanouchi S., Bonnoit J., Ghorbel A., “Response of the Knee Joint in Lateral Impact: Effect of Shearing Loads”, IRCOBI, 1990.

[6] Takahashi Y., Kikuchi Y., Konosu A., Ishikawa H., “Development and Validation of the Finite Element Model for the Human Lower Limb of Pedestrians”, Stapp Car Crash Journal, Vol. 44, 2000-01-SC22, 2000.

[7] “H-Dummy™ Version 1.6 User’s Manual”, Hankook ESI, Engineering Systems International, 1998.

[8] “Viewpoint Premier CATALOG”, 10th Anniversary Edition.

[9] Kajzer J. et al., “Shearing and bending effects at the knee joint at low speed lateral loading”, SAE paper #1999-01-0712, 1999.

[10] Kajzer J. et al, “Shearing and bending effects at the knee joint at high speed lateral loading”, SAE paper #973326, 1997.

[11] Beillas P., Begeman P. C., Yang K. H., King A. I.,

Arnoux P. J., Kang H. S., Kayvantash K., Brunet C., Cavallero C., Prasad P., “Lower Limb: Advanced FE Model and New Experimental Data”, Stapp Car Crash Journal, Vol. 45, 2001.
[12] Kajzer J., Cavallero C., Bonnoit J., Morjane, A., Ghanouchi S., “Response of the Knee Joint in Lateral Impact: Effect of Bending Moment”, IRCOBI, 1993.
[13] Woo S., Fox R., Sakane M., Livesay G., Rudy T., Fu F., “Biomechanics of the ACL: Measurement of In Situ Force in the ACL and the Knee Kinetics”, The Knee 5, 1998.
[14] Race A., Amis A., “The Mechanical Properties of the Two Bundled of the Human Posterior Cruciate Ligament”, Journal of Biomechanics, Vol 27(1), 1994.
[15] Fox R., Harner C., Sakane M., Carlin G., Woo S., “Determination of the In Situ Forces in the Human Posterior Cruciate Ligament using Robotic Technology - a Cadaveric Study”, The American Journal of Sports Medicine, Vol 26(3), 1998.
[16] Primal Pictures, “Interactive Knee Version 1.1”, 2000.
[17] A.D.A.M. Software, Inc., “A.D.A.M. Interactive Anatomy Version 3.0”, 1997.
[18] Pam System International, “PAM-CRASH™ PAM-SAFE™ Version 1998 Notes Manual”, 1998.
[19] Pam System International, “PAM-CRASH™ PAM-SAFE™ Version 1998 Reference Manual”, 1998.
[20] Mow V. C., Amoczky S. P., Jackson D. W., ed., “Knee Meniscus: Basic and Clinical Foundations”, New York: Raven Press, 1992.
[21] Kerrigan J. R., Bhalla K. S., Madeley N. J., Funk J. R., Bose D., Crandall J. R., “Experiments for Establishing Pedestrian-Impact Lower Limb Injury Criteria”, SAE Paper #2003-01-0895, 2003.
[22] Darvish K. K., Takhounts E. G., Mathews B. T., Crandall J. R., “A Nonlinear Viscoelastic Model for Polyurethane Foams”, SAE paper #1999-01-0299, 1999.
[23] Bose D., Sanghavi P., Kerrigan J. R., Madeley N. J., Bhalla K. S., Crandall J. R., “Material Characterization of Ligaments using Non-Contact Strain Measurement and Digitization”, International Workshop on Human Subjects for Biomechanical Research, 2002.